Bioelectrochemistry 149 (2023) 108324

Contents lists available at ScienceDirect

Bioelectrochemistry

journal homepage: www.journals.elsevier.com/bioelectrochemistry

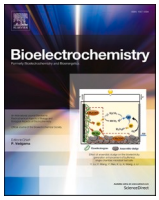

A novel comparative study for electrochemical urea biosensor design: Effect of different ferrite nanoparticles (MFe_2O_4, M: Cu, Co, Ni, Zn) in urease immobilized composite system

Vildan Sanko, Ahmet Şenocak *, Süreyya Oğuz Tümay, Erhan Demirbas *

Department of Chemistry, Gebze Technical University, Gebze 41400, Kocaeli, Turkey

ARTICLE INFO

Keywords:
Urea detection
Biosensor
Ferrite nanoparticles
Electrochemical sensing
conductive polymer

ABSTRACT

A new enzymatic electrochemical biosensor has been developed with the PANI/Nafion composite system containing ferrite nanoparticles with four different transition metals. The ferrite nanoparticles containing copper, cobalt, nickel, and zinc metals were synthesized by the co-precipitation method and their surfaces were modified with tetraethoxysilane and (3-aminopropyl) triethoxysilane to obtain $-NH_2$ function in order to develop the purposed sensing system. The modified and unmodified ferrite nanoparticles were characterized by physically, chemically, and morphologically. Ferrite nanoparticles with suitable for enzyme immobilization were integrated on the GCE surface and covered with PANI/Nafion. According toelectrochemical measurements, it was determined that copper ferrite nanoparticles, which have the lowest bandgap value, significantly increased the biosensor performance. Cyclic voltammetry (CV) and differential pulse voltammetry (DPV) were used to monitor biosensor production and evaluate its performance. A detection limit of 0.17 μM and a wide linear range of 0.5–45.0 μM were obtained for the urea detection with the DPV method with the sensing system (Nf/PANI/CuF/Urs). The biosensor has been successfully applied to soil and milk samples with high accuracy. In addition, it has been determined that the proposed method has good reproducibility, selectivity, and stability.

1. Introduction

Determination of urea concentration is extremely important in medical diagnosis as a potential indicator of kidney and liver dysfunction [1], as well as in food safety [2] and environmental control [3]. The presence of urea may cause a decrease in the pH value of the soil and thus a decrease in the yield of the grown plants [4]. Urea is an excellent example of an analyte with applications in a wide variety of fields, and due to the importance of monitoring urea levels in different fields, many types of urea biosensors using different transducer mechanisms have been demonstrated [5,6] such as amperometric [7], voltammetric [8], potentiometric [9], and optical [10] methods. Among them, voltammetric and amperometric methods include several advantages such as rapid measurement, linear response, good sensitivity and resistance to the influence of ionic strength [11]. There are currently available many methods such as headspace gas chromatography (HS-GC) [12], high-performance liquid chromatography with fluorescence detection (HPLC-FLD) [13] and gas chromatography-mass spectrometry (GC–MS) [14] for the determination of urea. However, these methods suffer from complex sample pretreatment and are not only expensive but also not suitable for in situ monitoring [12]. A sensitive, inexpensive and selective electrochemical biosensor can overcome these disadvantages due to their distinguished features such as low detection limit, specificity, simplicity of construction and ease of use [15,16].

Urease (Urs) is the enzyme for selectively reacts with urea, catalytically converting it to ammonium and bicarbonate ions [17,18]. The effectiveness of any urea biosensor depends on monitoring and effectively detecting the products obtained in the Urs-catalyzed reaction [19]. Products from the enzymatic hydrolysis of urea are not electrochemically active, so in most cases, different types of pH-sensitive redox mediators and conductive polymers are used to obtain an electrochemical signal [11,20]. Polyaniline (PANI) is one of the most frequently investigated as naturally conductive polymers for biosensor applications due to its good electrical conductivity, unique redox chemistry and biocompatibility [21,22]. In PANI-based urea biosensors, the electrochemical signal is generated by coupling PANI with NH_4^+ released by Urs during urea hydrolysis [11]. This system may often require the presence of Nafion (Nf) of the polymer to provide a

* Corresponding authors.
E-mail addresses: asenocak@gtu.edu.tr, erhan@gtu.edu.tr (E. Demirbas).

https://doi.org/10.1016/j.bioelechem.2022.108324
Received 10 July 2022; Received in revised form 7 November 2022; Accepted 8 November 2022
Available online 12 November 2022

terminated sulfonate group as a charge balancer in the medium [23]. Also copper [24], platinum [25] and gold [26] nanoparticles have been used to increase the catalytic property for NH_4^+ detection in the Nf/PANI system in the literature. Alternatively, in the current study, the contribution of the known catalytic effect of ferrite nanoparticles to the system was investigated. Thus, the effect of the differentiation of copper, cobalt, nickel, and zinc transition metals on the ferrite-based electrochemical urea system is investigated for the first time, which is supported for the positive contribution of ferrite nanoparticles to the sensitive and selective electrochemical urea biosensor. In addition, the contribution of the properties of four different ferrites to the peak current values has been examined in detail, and it is thought that the obtained outputs would create a new perspective for the design of future studies.

Ferrite nanoparticles are metal oxides with the general formula MB_2O_4, where M and B represent tetrahedral (region M) and octahedral (region B) regions in two different crystallographic domains. Here, M can be any metal with an oxidation state of + 2, such as Co^{2+}, Cu^{2+}, Mn^{2+}, Ni^{2+} and Zn^{2+} [27]. Cation types and their distribution in tetrahedral and octahedral regions have a very important effect on the physical and chemical properties of ferrite nanoparticles [28]. In addition, ferrite nanoparticles have attracted attention in numerous applications from industrial studies to medical applications because of their high effective anisotropy, oxidation resistance, magnetic properties, chemical stability and mechanical hardness [29–31]. In addition, it is known that ferrite nanoparticles make positive contributions in the field of bio/sensors [32,33]. Despite these good properties, ferrite nanoparticles have not been considered to use in any enzymatic electrochemical urea biosensor. We examined the contributions of ferrite nanoparticles containing different transition metals to biosensor performance by using the aforementioned positive properties of ferrites.

In this study, copper ferrite ($CuFe_2O_4$, CuF), cobalt ferrite ($CoFe_2O_4$, CoF), nickel ferrite ($NiFe_2O_4$, NiF) and zinc ferrite ($ZnFe_2O_4$, ZnF) nanoparticles were synthesized by co-precipitation method. Then, the surfaces of ferrite nanoparticles were modified with tetraethoxysilane (TEOS) and (3-aminopropyl) triethoxysilane (APTES). Thus, the surfaces of nanoparticles were made ready for enzyme immobilization by $–NH_2$ functionalization. Ferrite nanoparticles was functionalized both before and after modifications were characterized in detail with Fourier transform infrared (FTIR), X-ray diffraction (XRD), UV–vis absorption spectroscopies, scanning electron microscope (SEM), transmission electron microscope (TEM), and Zeta potential studies. Ferrite nanoparticles was coated separately on the Nf /PANI modified glassy carbon electrode (GCE) surface and the enzyme was immobilized on the surface of Nf/PANI/Ferrites/GCE (Nf/PANI/CuF/Urs, Nf/PANI/CoF/Urs, Nf/PANI/NiF/Urs, Nf/PANI/ZnF/Urs). Electrochemical measurements were performed with CV and DPV methods. The results obtained in the four synthesized ferrites were promising for detection of urea as expected, and the peak current values improved considerably compared to the system without ferrite nanoparticles. It was observed that the Nf/PANI/CuF/Urs nanocomposite exhibited the best performance for the electrochemical detection of urea. The required parameters of sensing systems such as repeatability, stability, reusability, selectivity, and real sample analysis (soil and milk) were performed with Nf/PANI/CuF/Urs electrode.

2. Experimental

2.1. Chemicals and reagents

Urease from Canavalia ensiformis (Jack bean), Type IX, powder, 50.000–100.000 units/g solid, glutaraldehyde solution (OHC$(CH_2)_3$CHO, 50 % w/v), aniline ($C_6H_5NH_2$, ≥99.5), 5 wt% Nafion® perfluorinated resin solution in lower aliphatic alcohols and water, copper chloride ($CuCl_2$, 97 %), cobalt(II) chloride hexahydrate ($CoCl_2{\cdot}6H_2O$, ≤ 100 %), nickel(II) chloride hexahydrate ($NiCl_2{\cdot}6H_2O$, 99.9 %), zinc chloride hexahydrate ($ZnCl_2{\cdot}6H_2O$, 99.9 %), sodium hydroxide (NaOH, ≥97.0 %), tetraethoxysilane ($C_8H_{20}O_4Si$, TEOS, ≥99.0 %), (3-aminopropyl) triethoxysilane ($C_9H_{23}NO_3Si$, 99 %), potassium dihydrogen phosphate (KH_2PO_4 ≥ 99.5 %), dipotassium hydrogen phosphate (K_2HPO_4>98 %), glucose ($C_6H_{12}O_6$, >96 %), uric acid ($C_5H_4N_4O_3$, ≥99.0 %), L-lactic acid ($C_3H_6O_3$, ≥98.0 %), ascorbic acid ($C_6H_8O_6$, >99 %), mercury(II) nitrate monohydrate ($Hg(NO_3)_2{\cdot}H_2O$, ≥98.5 %), lead(II) nitrate ($Pb(NO_3)_2$, ≥99 %), copper(II) nitrate monohydrate ($Cu(NO_3)_2{\cdot}H_2O$, 99.9 %), cadmium nitrate tetrahydrate ($Cd(NO_3)_2{\cdot}4H_2O$, 98 %), potassium hexacyanoferrate(III) ($K_3[Fe(CN)_6]$, ≥99.0 %), potassium hexacyanoferrate(II) trihydrate ($K_4[Fe(CN)_6].3H_2O$, ≥99.0 %) were obtained from Sigma-Aldrich, USA. Iron(III) chloride hexahydrate ($FeCl_3{\cdot}6H_2O$, 97 %), methanol (CH_3OH, ≥99.9 %), toluene (C_7H_8, ≥99.9 %) ethanol (CH_3CH_2OH, absolute), solution of ammonium hydroxide (NH_4OH, 30–33 %) were obtained from Merck, Germany.

2.2. Characterization methods

Powder XRD (Rigaku, Japan) was used to assess the crystal structures of CuF, CoF, NiF, ZnF nanoparticles. FTIR measurements (Perkin Elmer, USA) were recorded at a resolution of 4 cm^{-1} per second for 16 scans to support the structural analysis of materials. Surface morphological characterization were observed with SEM (FEI-Nova) after with palladium-gold-coating thin film. TEM images were obtained with the Hitachi (HT-7700, Japan). Optical absorption spectra of ferrite nanoparticles were calculated using T80 + UV–vis spectrometer (PG Instruments ltd, UK) to find band gap energies. Also, the surface charges of ferrite nanoparticles were calculated using a Malvern Zetasizer Nano-ZS (Malvern Instrument, UK) in 0.05 M phosphate buffer at pH 7.0. CV and DPV methods were used for electrochemical measurements with CH Instruments CHI440B (USA) at room temperature.

2.3. Synthesis of MFe_2O_4 nanoparticles

In this study, the "co-precipitation" method, which consists of precipitation of an aqueous solution including inorganic salts in the appropriate stoichiometry by increasing the pH, was preferred for obtaining the ferrite nanoparticles. Initially, the solutions of $FeCl_3{\cdot}6H_2O$ and $CuCl_2$, $CoCl_2{\cdot}6H_2O$, $NiCl_2{\cdot}6H_2O$, and $ZnCl_2{\cdot}6H_2O$ salts were prepared in distilled water by calculating their 2:1 ratio in moles. Two solutions ($FeCl_3{\cdot}6H_2O$ and + 2 valence metal salts solutions) placed in the round bottom flask was mixed for about 10 min at a constant stirring speed (200 rpm) and at room temperature. Then, 0.5 M NaOH solution was added dropwise to the reaction mixture until pH value of the mixture was reached to 11.0 [34]. While the mixing process continued, brown-black precipitate formations were observed with the addition of NaOH. After the desired pH value was obtained, the solution temperature was kept at 80 °C and stirred for about 2 h. After this process, the mixture was allowed to cool to room temperature and the obtained particles were washed 3 times with distilled water and collected by centrifugation (4000 rpm). As a final step, the obtained products were dried in an oven at 100 °C for one day and then calcined in a furnace at 750 °C for 6 h.

2.4. TEOS and APTES modifications of MFe_2O_4 nanoparticles

The surface functionalization of nanoparticles is an important step in material design because the appropriate functionality determines the end-use and provides control of the physicochemical processes on the surface. Thus, it adjusts various magnetic, optical and electrical properties in the desired direction. Silanization processes were applied to obtain nanomaterials with more uniform morphology to reduce agglomeration and to have the $–NH_2$ functional group for Urs immobilization. The same procedure was applied for each modification of CuF, CoF, NiF and ZnF nanoparticles with TEOS and APTES. First of all, 0.25 g of each ferrite nanoparticle was weighed for the TEOS modification and

dispersed in anhydrous ethanol for about 1 h with the help of a sonicator. Ammonium hydroxide solution (4.5 mL) and TEOS (2.0 mL) were added to the resulting homogeneous dispersion. The final mixture was continued to be mixed with a magnetic stirrer at room temperature for 12 h. The TEOS modified products were washed with distilled water and ethanol, respectively and they were obtained by precipitation by centrifugation (4000 rpm) [35]. Modified ferrite nanoparticles (CuF-TS, CoF-TS, NiF-TS, ZnF-TS) dried in an oven at approximately 60–70 °C were stored in glass vials for characterization and subsequent steps. Since ferrite nanoparticles modified with TEOS didn't have functional groups for immobilization Urs, APTES modification was carried out to structure for having $–NH_2$ functional group. In order to obtain APTES-functionalized particles, CuF-TS, CoF-TS, NiF-TS, and ZnF-TS materials (0.1 g) were weighed and dispersed in anhydrous toluene and APTES (2.0 mL) was added into the dispersion. The reaction mixture was refluxed at 100 °C for 16 h and APTES-modified products (CuF-TS/AS, CoF-TS/AS, NiF-TS/AS, ZnF-TS/AS) were washed with toluene and ethanol. The final APTES-modified products were precipitated by centrifugation at 4000 rpm and they were dried in an oven at approximately 60–70 °C [36].

2.5. Electrochemical parameters and electrode modification

Electrochemical studies were carried out with a three-electrode system. The modified GCE (3.0 mm in diameter) was used as the working electrode while platinum wire and Ag/AgCl (3.0 M KCl) electrodes were used as counter and reference electrodes, respectively. All electrochemical measurements were taken in 0.5 M PBS at a pH of 7.0. CV measurements were performed a scan rate of 100 mV s^{-1} between −0.6 and 1.0 V. DPV curves were recorded from −0.6 to 0.8 V at a pulse period of 1.0 s, an amplitude of 0.2 V and a pulse width of 0.01. Experiments were performed in triplicate . Before modification of the working electrode, the GCE surface was polished with alumina slurries of different thicknesses (0.1 μm, 0.05 and 0.03 μm) and washed with distilled water and ethanol. The procedure for the modified working electrode is as follows; The 5.0 % Nf solution was diluted with ethanol to obtain 1.0 % solution and 1.5 μL was dropped onto the cleaned GCE and dried at room temperature. Then, aniline solution (0.1 M (aniline): HCl (1.0 M)) was polymerized on the Nf-coated GCE surface. The polymerization was carried out in the range of −0.3–1.0 V using the CV method for three cycles and the scanning rate was 0.05 V. After the electrochemical polymerization process, the electrode surface was washed with distilled water to remove the nonbinding monomers and allowed to dry at room temperature. A dispersion of 2.0 mg mL^{-1} of TS/AS modified ferrite nanoparticles were prepared in distilled water, and 3.0 μL of these dispersions were dropped onto the Nf/PANI coated GCE surface. Finally, glutaraldehyde was added to 6.0 mg mL^{-1} Urs solution as a cross linker in 0.5 M PBS at pH 7.0, and 10.0 μL of the prepared solution was dropped onto the electrode surface to immobilize the enzyme. After the electrode surface was completely dry at room temperature for 2 h, unbound enzymes and crosslinkers were removed by washing with distilled water.

2.6. Preparation of real samples

A milk sample was obtained from the rural area of Kocaeli, Turkey for electrochemical quantification of urea by the DPV method. Electrochemical parameters were used in the same way as optimized for urea detection in the buffer system in real sample analysis. Milk samples were diluted 1000 times with 0.5 M PBS (a pH of 7.0) without any pretreatment. The amount of urea in the milk was determined by adding of milk sample to the measurement cell after DPV baseline was fixed.

For the determination of urea in the soil sample, 1.0 g soil sample was weighed and sonicated in 20 mL distilled water for half an hour. The mixture was collected by centrifugation at 4000 rpm [37]. The electrochemical measurements of the sample were recorded with DPV, which was diluted 1000 times with 0.5 M at a pH of 7.0 PBS. The accuracy of the biosensor was investigated by spike and recovery test at two different concentrations (5.0 and 7.5 μM).

3. Results and discussion

3.1. Characterization of MFe_2O_4 and silane modified MFe_2O_4 nanoparticles

XRD patterns were used to gain detailed information for the crystal structures different transition metals containing ferrite nanoparticles. The obtained results are given in Fig. 1**a** and the characteristic peaks of ferrite nanoparticles are marked in the figure. The peaks at 2θ at 33.36, 35.58, 38.76, 44.02, 49.8, 54.08, 62.84°supported the tetragonal spinel $CuFe_2O_4$ values (ICDD Card no: 00–072-1174) [32]. The corresponding peaks values of 18.18, 30.08, 35.73, 43.26, 57.24, 62.98°at the 2θ value supported the cubic spinel $CoFe_2O_4$ values (ICDD Card no: 00–003-0864) [38]. The peaks values of 2θ at 30.0, 35.5, 37.1, 43.1, 57.5 and 62.3°supported the cubic spinel $NiFe_2O_4$ values (ICDD Card no: 00–054-0964) [39]. The peaks of 2θ at 30.2, 35.4, 43.2, 58.8 and 62.2°supported the values of cubic spinel $ZnFe_2O_4$ (ICDD Card no: 00–022-1012) [40]. The crystallite sizes of the samples were calculated using the Scherrer equation using the values obtained from the X-ray diffraction spectra [41]. Crystal sizes were calculated for the 35° peaks obtained from the XRD spectra for each sample. Average crystallite sizes were calculated as 25.42 nm, 44.71 nm, 21.63 nm, and 27.88 nm for CuF, CoF, NiF, ZnF, respectively.

FTIR analysis was also performed for the chemical characterization of ferrite nanoparticles after the calcination processes. In general, the base metal–oxygen bonds of all ferrites was monitored in the range of 400–600 cm^{-1} corresponded to the vibration of the metal–oxygen bond in the octahedral and tetrahedral regions, respectively [42]. The FTIR spectra of the ferrite nanoparticles are given in Fig. 1**b**, and the peaks belonging to the tetrahedral and octahedral regions were observed between 400 and 600 cm^{-1}. These peaks were characteristic for metal–oxygen bonds confirmed for the fabrication of ferrite nanoparticles. FTIR analysis was also performed for the chemical characterization of TEOS, and APTES modified ferrite nanoparticles (**Fig S1 and** Fig. 1**c**). In the spectra of TEOS modified ferrites, the presence of Si-O-Si bonds was observed clearly at approximately 1000 cm^{-1} (Fig. S1) [43]. No peak was observed in this region in the FTIR spectra of unmodified ferrite nanoparticles. Therefore, it was clearly concluded that silica was modified on the ferrite nanoparticle surfaces. The vibrations of the propyl group on APTES were observed in the FTIR spectra of the nanoparticles after the modification process with APTES, the C—H stretching vibrations at 2930 cm^{-1}. In addition, vibrations at 3510 cm^{-1} and 1560 cm^{-1} could be associated with N—H stretching and bending [36].

SEM micrographs were analyzed to understand the morphologies of the ferrite nanoparticles (**Fig S2**). SEM images showed that ferrites had agglomeration intensively due to their magnetic properties and small particle size (**Fig. S2a-d**) [44,45]. In addition, it was observed that the grain shapes were irregular due to the grinding process after calcination. Irregular grain shapes were more clearly observed with TEM (Fig. 2**a-d**). SEM images of APTES and TEOS modified ferrites (CuF-TS, CoF-TS, NiF-TS, ZnF-TS) were obtained and the results are given in **Fig. S2e-h**. It was expected to obtain spherical nanoparticles by silanization of TEOS and to partially prevent agglomeration. According to the SEM images, the purposed target was obtained with this modification. As could be seen from TEM images of TEOS modified ferrites, it is observed that all ferrites had spherical morphology. It was seen that the surfaces of spherical structures were smooth, and their dimensions were homogeneous (Fig. 2e-h). Gao et al., in 2011 modified Fe_3O_4 nanoparticles and obtained spherical structures after modification with TEOS [46]. Moreover, the agglomeration of Fe_3O_4 nanoparticles was caused by the drying process, reduced agglomeration of spherical nanoparticles could

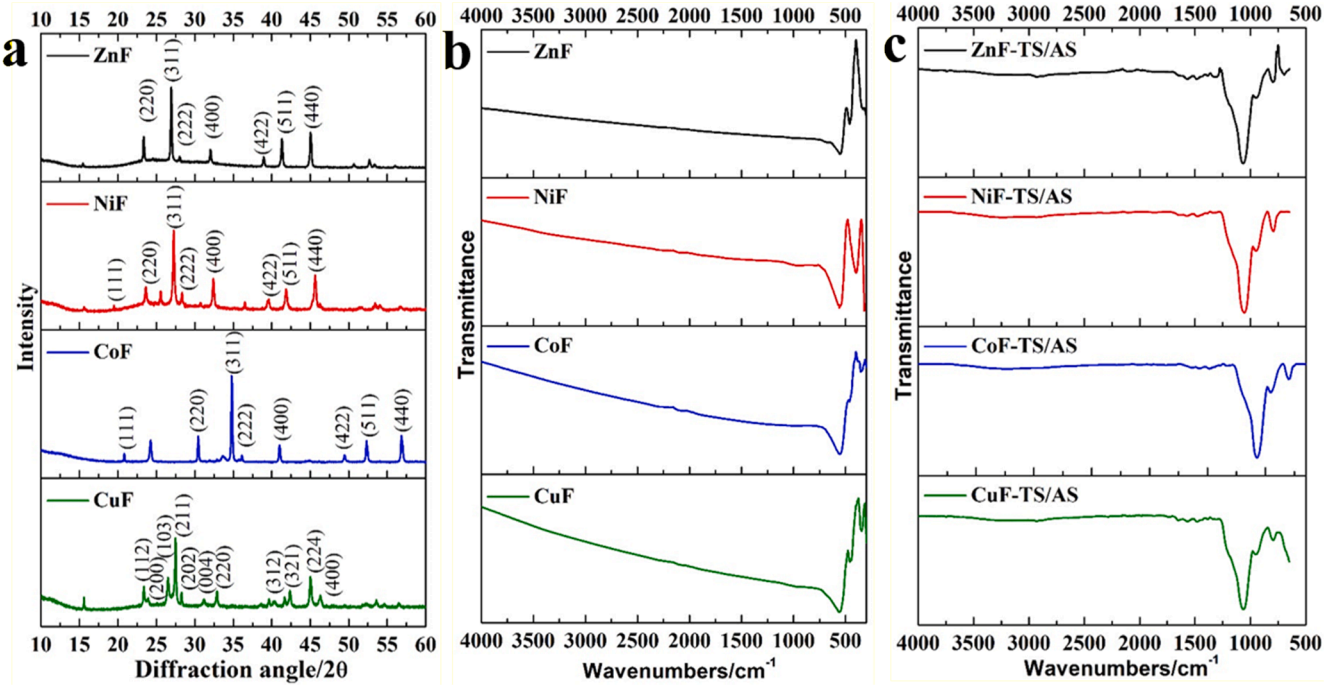

Fig. 1. (a) XRD, (b) FTIR spectra of CuF, CoF, NiF, ZnF, and (c) FTIR spectra of CuF-TS/AP, CoF-TS/AS, NiF-TS/AS and ZnF-TS/AS.

be obtained with TEOS functionalization [47]. After the modification with APTES, it was observed that there was no change in the morphology that could be noticed from the SEM images (Fig. S2**i-l**). The difference in morphology of TEOS and APTES modified ferrite nanoparticles (CuF-TS/AS, CoF-TS/AS, NiF-TS/AS and ZnF-TS/AS) is obviously proven from the TEM images (Fig. 2**i-l**). After the modification with APTES, it was observed that the shell structure was formed in different thicknesses. These changes also supported the modifications of ferrite nanoparticles.

Nanoparticle surface charge density plays an important role in many applications. When a particle is immersed in an aqueous medium, it becomes charged due to protonation/deprotonation at the particle surface. The resulting surface charge interacting with the dissolved ions form the electrical double layer surrounding the charged particle [48]. In this study, the surface charge properties of synthesized four different ferrite nanoparticles were analyzed with their Zeta potential values. Measurements were recorded by suspension in 0.05 M PBS a pH of 7.0 at 25 °C. Three replicates were made for each sample to determine the error in the measurements. The resulting surface charges were calculated as −30.8 ± 1.34 mV, −29.27 ± 1.85 mV, −30.33 ± 1.30 mV, –33.34 ± 1.42 mV for CuF, CoF, NiF and ZnF, respectively. It was determined that there was no significant differences between the surface charges. Therefore, it was thought that the difference between the peak current values was due to the bandgap.

The optical behavior of the synthesized nanomaterials was investigated by UV–vis spectroscopy between 200 and 1000 nm (Fig. 3). Absorbance depends on many factors such as grain size, bandgap, surface roughness and lattice parameters. It exhibits relatively narrow bandgap, superior conductivity and beneficial properties to promote electron transfer [49]. Therefore, UV–vis analysis contains very important features for this study. The energy band gap values of all samples were calculated using the Tauc plot [50]. The bandgap values of CuF-TS/AS, CoF-TS/AS, NiF-TS/AS and ZnF-TS/AS nanoparticles were calculated as 1.25, 1.56, 2.14 and 2.40 eV, respectively. When ferrite nanoparticles were evaluated in terms of sensitivity to urea in the electrochemical biosensor system, it was determined that there was a linear relationship with the obtained band gap. The valence band and conduction band positions of the ferrite nanoparticles are calculated from the following Equations 1 and 2;

$$E_{VB} = X - E_e + 0.5E_g \quad (1).$$

$$E_{CB} = E_{VB} - E_g \quad (2).$$

where E_{CB}, E_{VB}, X, E_g and E_e are the conduction band, valence band energy of the semiconductor, geometric mean of the electronegativity of the constituent atoms in the semiconductor, bandgap energy and energy of free electrons with a constant value of 4.5 eV against NHE on the hydrogen scale [50]. E_{CB} values of CuF-TS/AS, CoF-TS/AS, NiF-TS/AS and ZnF-TS/AS were calculated as 0.019 eV, −0.218 eV, −0.458 and −0.588 eV, respectively. In addition, E_{VB} values were determined as 1.269 eV, 1.342 eV, 1.682 and 1.812 eV. The numerical data is shown in **Fig S3.**

3.2. *Optimization of experimental parameters*

In order to obtain the best performance of new designed biosensor for urea detection by electrochemical method, Nf volume, PANI cycles, amount of ferrite nanoparticle, Urs concentrations and immobilization times were optimized. Optimization studies were carried out by immobilizing 2.0 mg mL^{-1} of Urs enzyme in all control groups because any enzyme-free control group did not respond to urea. The peak current values obtained from the CV measurements are presented in **Fig S4**. Although, amounts of Nf (0.5, 1.0, 1.5, 3.0, 5.0 μL) were investigated in different volumes on the surface of the cleaned GCE electrode, CV responses demonstrated for negligible changes. As seen in **Fig. S4a**, the optimum Nf volume was determined to be 1.5 μL. In the second optimization step, PANI was electrochemically polymerized on 1.5 μL Nf containing GCE in 5 different cycles among 2 and 8. It was observed in Fig. S4**b** that 3 cycles of PANI gave the highest peak current value and thus it was determined as the optimum cycle but when the number of cycles for electropolymerization of PANI exceeds three, lower biosensor performance was observed due to weakening the connection between the electrode surface and the solution. In the third step, CuF solutions prepared at 5 different concentrations (0.5, 1.0, 1.5, 2.0, 4.0 mg mL^{-1}) were dropped onto the electrode surface containing 1.5 μL Nf and 3 cycles of PANI. It was observed that ferrite nanoparticles showed higher peak current value at 2.0 mg mL^{-1}, but the peak current was significantly reduced at smaller and higher concentrations (Fig. S4**c**). In the

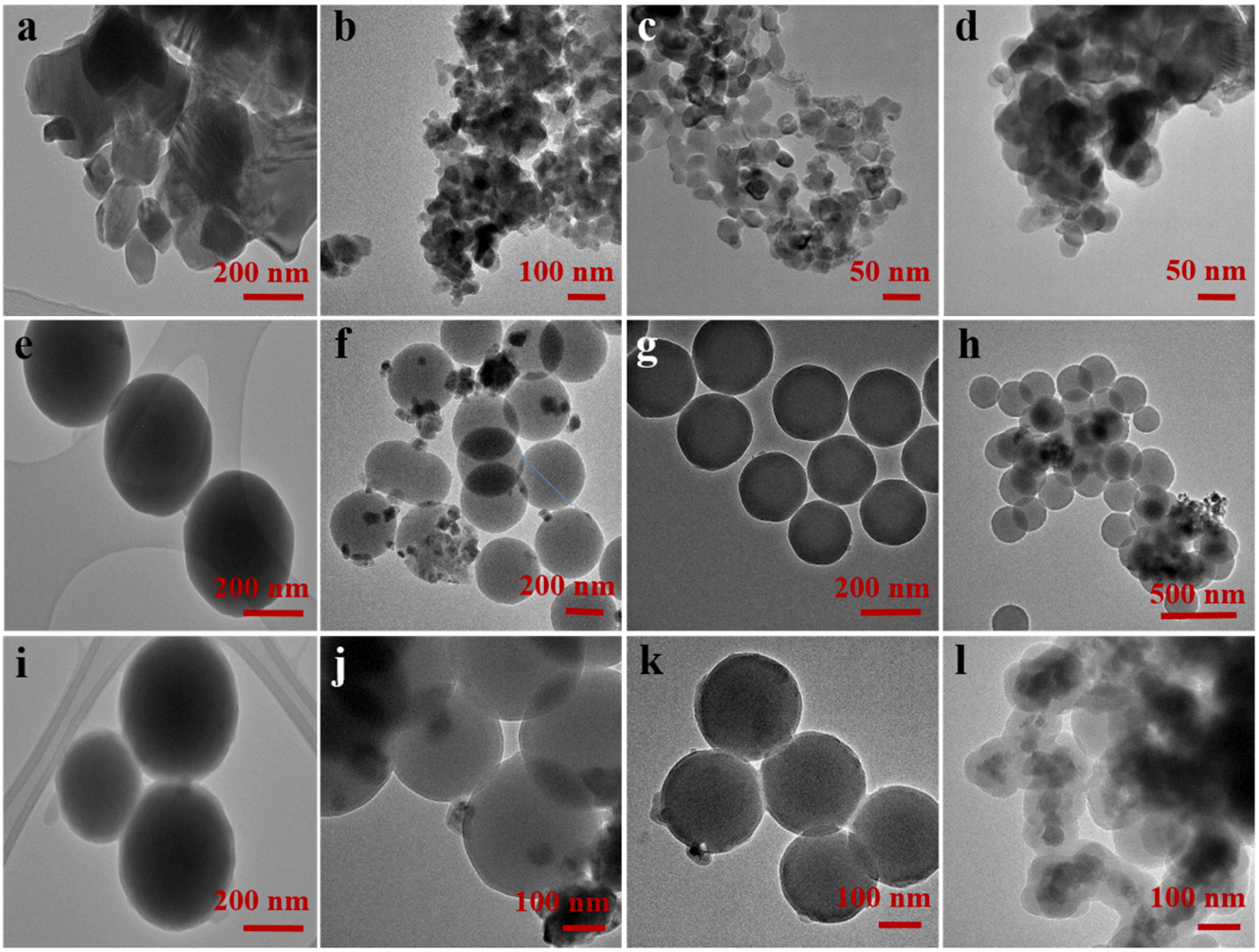

Fig. 2. (a) TEM images of CuF, (b) CoF, (c) NiF, (d) ZnF, (e) CuF-TS, (f) CoF-TS, (g) NiF-TS, (h) ZnF-TS, (i) CuF-TS/AS, (j) CoF-TS/AS, (k) NiF-TS/AS and (l) ZnF-TS/AS.

fourth step, enzyme concentration was tested as 4.0, 6.0, 8.0, 10.0 mg mL^{-1} under the optimized conditions. The optimum enzyme concentration was found as 6.0 mg mL^{-1} because of steady increase in the electrochemical response of the new urea biosensor (Fig. S4**d**). In the final optimization step, CV measurements were taken against the analyte at the same concentration at different times after immobilizing the electrode surface with the enzyme. It took approximately 2 h for the electrode to fully dry under room conditions. For this reason, measurements were made at 5 different times; 2, 4, 6, 8 and 10 h. Since there was no significant difference between the immobilization times of 2 h and 10 h. 2 h, which is the time when the electrode surface was completely dry, was accepted as optimum (Fig. S4e). All parameters were optimized and the determined values were used in all further biosensor studies.

3.3. Electrochemical characters of the biosensors

The synergistic contribution of the synthesized ferrite nanoparticles for the determination of the urea was investigated with addition of ferrite nanoparticles after optimization of Nf/PANI system. The voltammograms given in Fig. 4**a** showed the contribution of components of the designed biosensor to the sensor performance. It is clearly observed that Nf or PANI system showed none voltammetric response even if the enzyme was immobilized. In addition, when they are combined with the enzymatic sensor system, peak response was very small against to urea. Importantly, it was determined that the addition of ferrite nanoparticles into Nf/PANI system had a very positive contribution to the peak current value. Also, Nf is indispensable in the composite prepared for the enzymatic urea detection mechanism in this study. It was observed that the Nf-free electrode surface did not give an electrochemical response in the presence of urea. However, if there was no enzyme in this system, an electrochemical reaction against urea could not be obtained. Ultimately, it is clear that the biosensor mechanism runs through the enzymatic system. CVs responses of ferrite nanoparticles and sensing electrode without ferrite against urea at the same concentration are shown in Fig. 4**b**. When voltammogram of the system was examined without ferrites, the lowest peak current value was observed. The ZnF containing system gave approximately 2 times higher peak current values than Nf/PANI/Urs at the same concentration of urea. It was determined that the NiF containing system demonstrated approximately 3 times higher the peak current values, while the systems containing cobalt and copper ferrite showed approximately 6 and 7 times higher the peak current values according to non-ferrite biosensor system. In addition, there were some changes in the potential values of the electro oxidation peaks of urea. The oxidation peak of the ferrite-free system was observed at 0.33 V for non ferrit system, at 0.30 V for CuF, at 0.30 V for CoF, at 0.31 V for NiF and at 0.32 V for ZnF. In this case, it was concluded that the ferrites showed a catalytic effect as expected. At the same time, the highest peak current value was determined with the CuF containing system. Although, it was mentioned in the literature that nickel-based catalysts exhibited excellent catalytic abilities for urea oxidation, especially in non-enzymatic systems [51,52], such a generalization for enzymatic

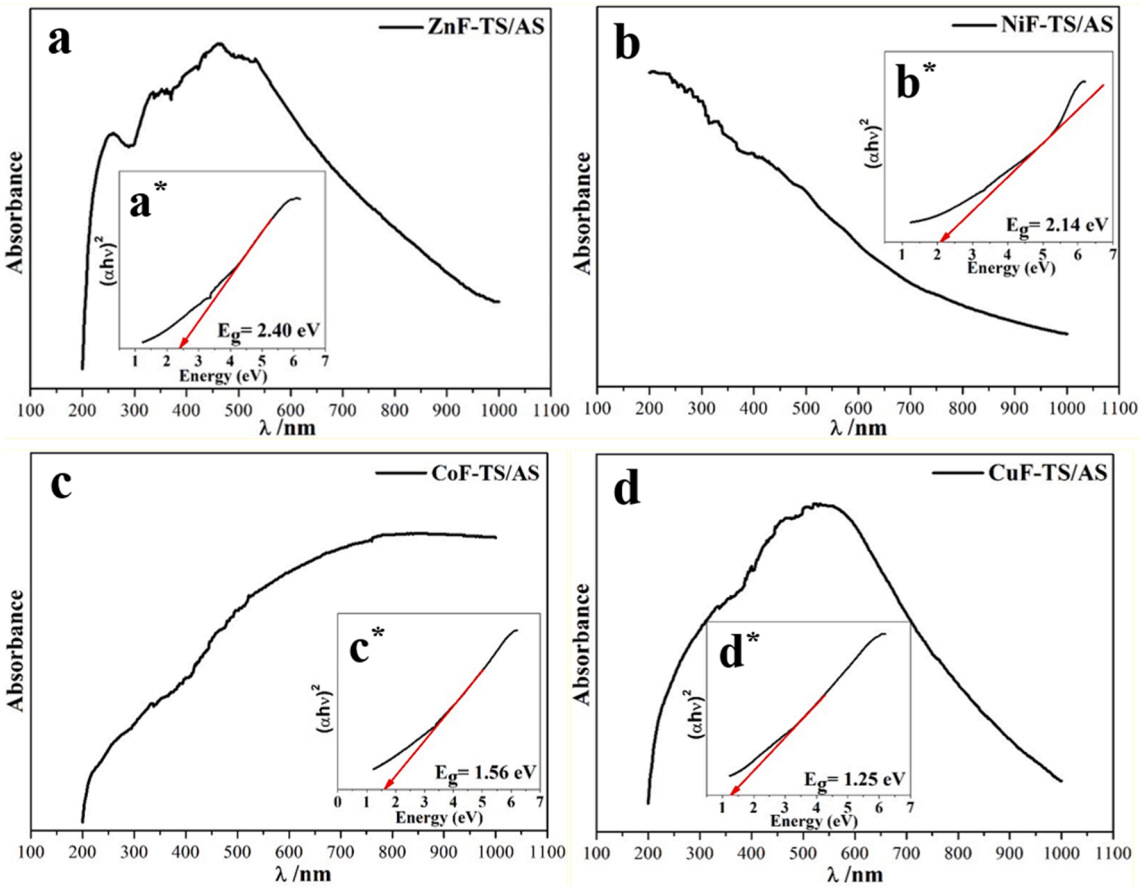

Fig. 3. Absorption spectra (a-d) and Tauc plots (a*-d*) of synthesized CuF-TS/AS, CoF-TS/AS, NiF-TS/AS, and ZnF-TS/AS.

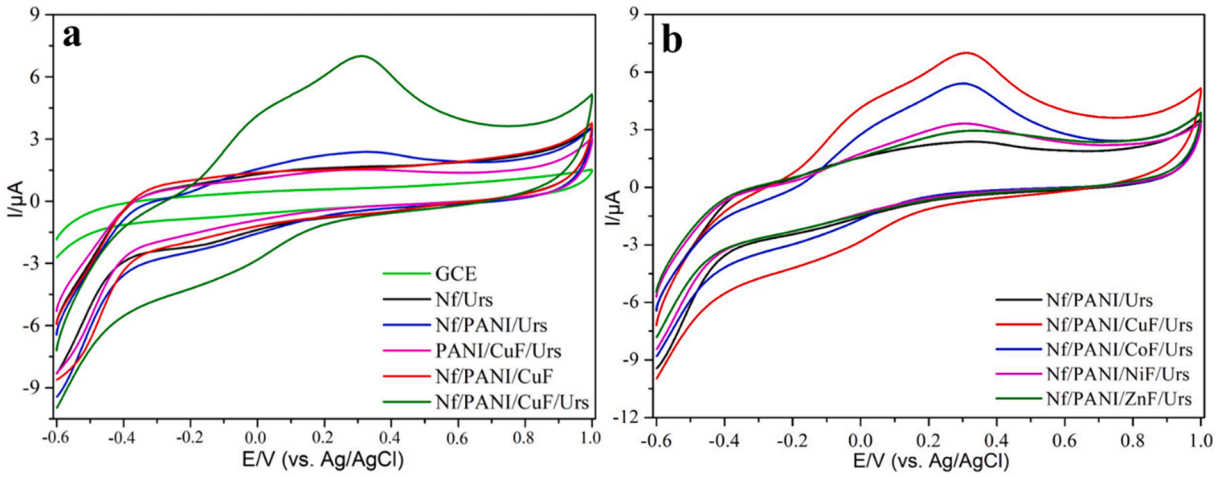

Fig. 4. CV responses of different groups at 0.5 M PBS (a pH of 7.0).

systems may not be correct because a wide variety of nanoparticles have been designed in the literature for enzymatic urea biosensors [53,54].

A schematic illustration of Nf/PANI/CuF/Urs based biosensor preparation procedure and the detection mechanism for NH_4^+ which is the product of enzymatic degradation of urea is given in Scheme 1. As known, Urs reacts with urea catalytically converting it to ammonium and bicarbonate ions that have crucial effect of any urea biosensor. The products obtained by enzymatic hydrolysis of urea were not electrochemically active and a second enzyme or metal electro catalysts could be used to oxidize the NH_4^+ ion to generate an electrical signal. Srivastava et al. developed an amperometric urea biosensor using urease and glutamate dehydrogenase simultaneously for the electrochemical oxidation of ammonia. However, the use of binary enzymes increased the complexity of sensor design and increased the cost/performance ratio [55]. Various conductive polymers such as polypyrrole [56], polyaniline [8] and poly(3,4-ethylenedioxythiophene) [57] were used for urea sensors. The electrochemical signal was generated by coupling PANI with NH_4^+ released by Urs during hydrolysis of urea in PANI based urea biosensors. However, detection of cationic NH_4^+ with PANI may require modification of the polymer with Nf to provide a terminated sulfonate group as a charge stabilizer during doping/de-doping process. Therefore, initially, the emeraldine state of PANI has a positively

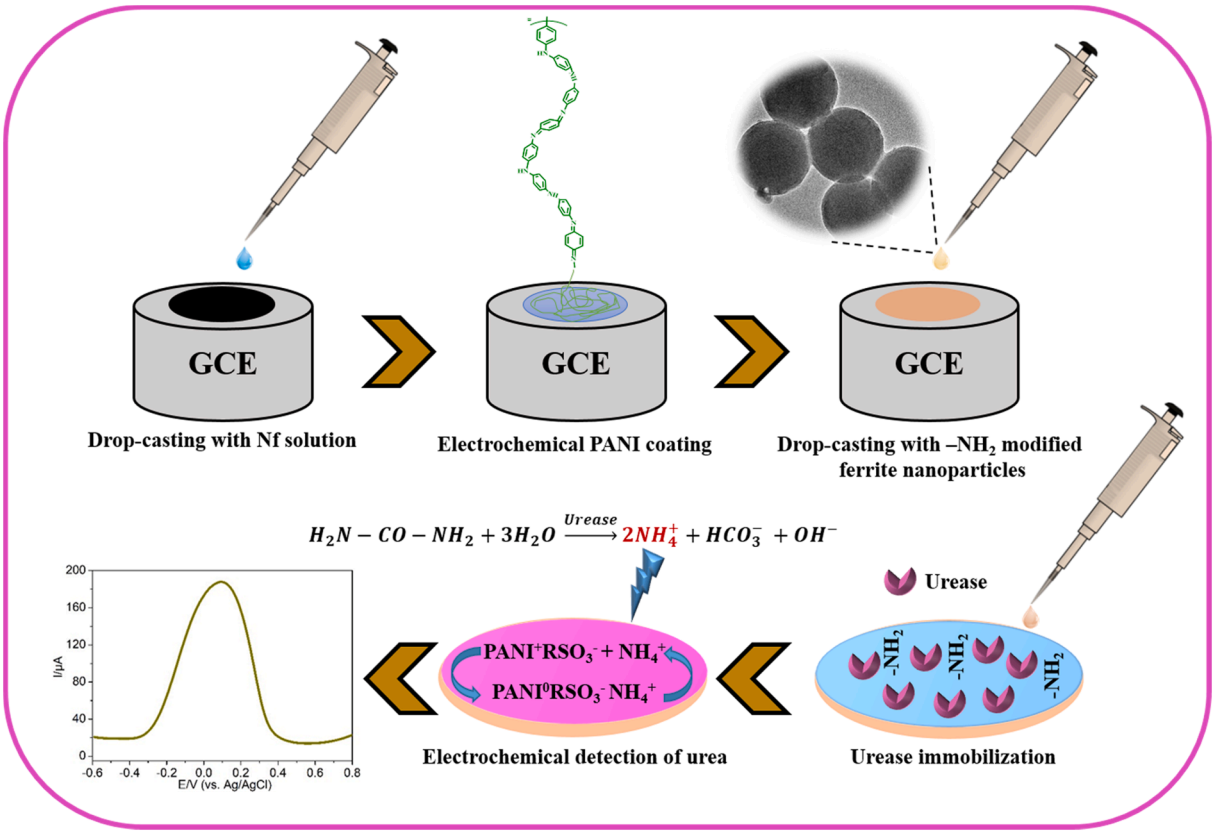

Scheme 1. Nf/PANI/CuF/Urs biosensor preparation procedure and a schematic illustration of NH_4^+ detection mechanism and the product of enzymatic degradation of urea.

charged backbone, and the negatively charged Nf serves as an inactive poly-anionic charge stabilizer within the polymer matrix [11]. In addition, for the quantitative determination of NH_4^+ with the PANI:Nf electrode, it could be concluded that the anodic and cathodic currents will gradually increase as the NH_4^+ concentration increases. In addition, a large number of metal oxide nanoparticles [58,59], carbon materials [60,61] and dots [62,63] have good electron transfer properties, sensitivity and large effective surface area, which can lead to shorter response and higher sensitivity. Among them, ferrite nanoparticles are of interest in various application areas ranging from industrial studies to biomedicine because of their high effective anisotropy, magnetic properties, mechanical hardness, chemical stability and oxidation resistance [30,64]. However, they have not yet been used in a system for electrochemical urea detection. For this reason, the effect of ferrite nanoparticles exhibiting four electro-catalytic properties was investigated in the current study. **Fig S5** shows the CV voltammograms in the presence of urea at different concentrations. It was observed that the peak currents gradually increased as the urea concentration increasesed for the quantitative detection of NH_4^+ in all electrodes containing ferrite nanoparticles. LOD values obtained at 2.0–45 μM linear range from the CV curves were calculated as 6.4 μM, 7.7 μM, 12.2 μM and 13.3 μM for CuF, CoF, NiF and ZnF containing systems, respectively.

The DPV graphs obtained by adding the synthesized ferrite nanoparticles to the Nf/PANI composite are given in Fig. 5 **and Fig S6**. The peak current values for all four ferrites were higher than the Nf/PANI modified GCE. LODs obtained from the DPV were calculated as 0.17 μM,

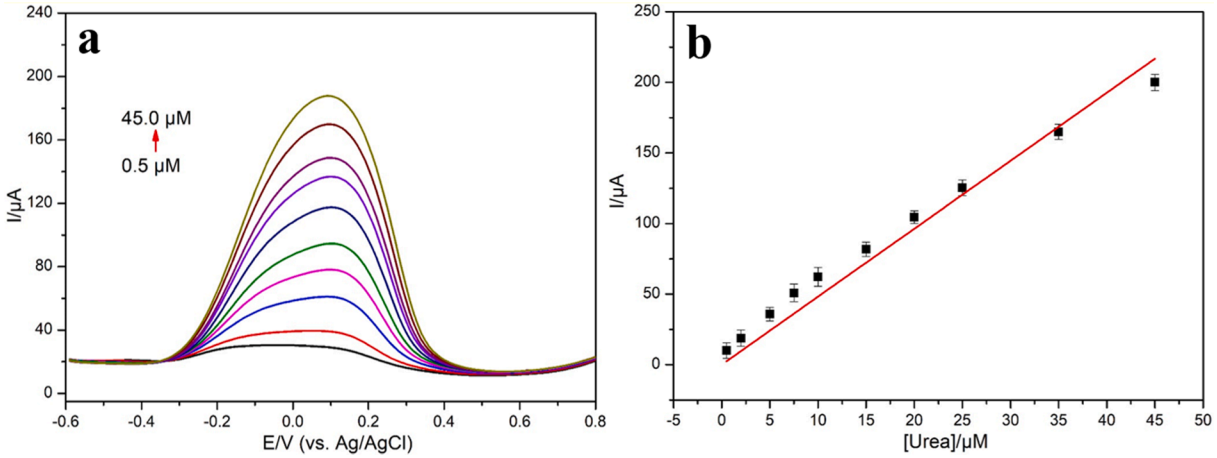

Fig. 5. DPV responses for different concentrations of urea on Nf/PANI/CuF/Urs and (b) the linear relationship between currents and concentrations of urea.

0.23 μM, 0.37 μM and 0.42 μM according to the peak current values for CuF, CoF, NiF and ZnF containing systems, respectively. The LOQ for CuF, CoF, NiF and ZnF modified sensors for the same ranking were determined as 0.56 μM, 0.76 μM, 1.22 μM and 1.39 μM. The linear measurement range was determined as 0.5–45 μM for all four ferrite nanoparticles. Further analytical studies were carried out with CuF due to its lower LOD value and higher sensitivity. The peak current values of the voltammetric measurement results were determined as order of CuF > CoF > NiF > ZnF from largest to smallest. It was thought that the difference in the electrochemical response may be due to the surface charge of the ferrites or the bandgap values, depending on the detected ion. Therefore, band gap values are noteworthy because there was no significant difference in the surface charges of ferrite nanoparticles. Since CuF exhibited relatively narrow band gap, superior conductivity and beneficial properties to promote electron transfer [49]. Band gap values were calculated with the data from UV-Vis absorbance measurements to support this idea and the band gap energy values of all samples were calculated using the Tauc plot. The band gap values of CuF, CoF, NiF and ZnF were calculated as 1.25, 1.56, 2.14 and 2.40 eV, respectively. When ferrite nanoparticles were evaluated in terms of sensitivity to urea in the new electrochemical biosensor system, it was determined that there was a linear relationship with the obtained band gap. Dhinasekaran et al. developed a hybrid CuO/ZnO and Fe_2O_3/ZnO nanostructures modified graphite electrode for the urea sensor. The results indicated that the Fe_2O_3/ZnO coated graphite electrode with the lowest bandgap value showed a higher response to urea than the others [65].

It was determined that the LOD value was significantly lower than the literature studies close to the designed new biosensor (Table 1) [11,26,65–68]. In addition, a wide linear measurement range could increase its potential usage area. The study of Uzunçar et al. was evaluated as comparable to this study because of both the content of the study and its up-to-date nature in which nanofibrous polyaniline: polystyrene-sulfonate was designed and reported as a functional composite for enzyme-linked urea biosensors. They specified the linear measurement in the range from 0.2 to 0.9 mM, and the LOD value was 51.8 μM. As compared to this study, it was noticed that the reference study had both a rather narrow operating range and a high LOD value [11]. Singh et al., used Fe_3O_4/MWCNT-polyaniline nanocomposite for urea detection and found the linear measurement range as 1.0–25.0 mM, and the LOD value was 67.0 μM [8]. The obtained data showed that the designed new urea biosensor was comparable with the studies in the field. Therefore, the advantages of the new developed electrochemical urea biosensor has low LOD, wide linear measuring range, selectivity, relatively low cost, and easy preparation process.

3.4. Repeatability, stability, reusability, lifetime and selectivity analysis

The -RSD% value of the CuF composite system in the 15.0 μM urea containing PBS was calculated according to the results of 10 consecutive measurements **(Fig S7)**. As a result of the calculations, the RSD% value was 2.07 % which was considered successful for sensor performance (<5%).

For to test the reproducibility of the biosensor, the DPV responses of four biosensors (Nf/PANI/CuF/Urs) immersed in the measurement medium including 10.0 μM urea were recorded and analyzed. A good RSD value of 2.88 % was obtained for the biosensor indicating good reproducibility. The voltammograms are shown in **Fig S8**.

DPV measurements were performed on the same electrode to determine the reusability of the biosensor (Nf/PANI/CuF/Urs). As seen in **Fig S9**, after the first DPV measurement in the presence of 5.0 μM urea, the surface of the electrode was gently washed with distilled water and keep to dry at room temperature. This process was repeated 4 times and the relative error for the peak current values were calculated in the first three measurements as 1.57 %. However, after the fourth measurement, decreasing of peak current was found to be 72.2 %. It could be stated that this situation was caused by deformation of the electrode surface and decreased in the enzyme activity.

In order to determine the lifetime of the existing biosensor, measurements were taken at the same concentration (25.0 μM) at five different times within a month. The measurements were repeated at least three times. The electrodes were kept at room conditions and placed on a stand with their surfaces open to air. The durations were determined as 1st day, 3rd day, 7th day, 15th day and 30th day. The graph of the peak current values obtained is given in the Supplementary data as Figure S10. In the electrochemical measurements taken up to the 7th day, no significant difference was observed in the response of the biosensor to the same concentration of urea, and it was calculated as about 1.5 %. However, on the 15th day, a decrease of 14.28 % in the peak current value was observed, and on the 30th day, 30.51 % compared to the first day. As a result, it was determined that the designed new electrochemical urea biosensor gave accurate results within the first 7 days. The decrease observed in the peak current value after the 7th day could be attributed to the decreased activity of the enzyme [69].

The selectivity of the presented urea biosensor (Nf/PANI/CuF/Urs) was investigated to evaluate the effect of various interfering agents such as uric acid, glucose, ascorbic acid, lactic acid, Hg^{2+}, Cd^{2+}, Pb^{2+}, Cu^{2+}. Firstly, 50 eqv. of interference agents was added to PBS and analyzed by the DPV in absence of urea, and no peak formation was observed. Then, the peak current value was determined by adding 7.5 μM urea into the medium (Fig. 6**a**). Finally, the DPV measurement was recorded with

Table 1
Comparisons of electrochemical urea biosensors.

Working Electrode	Technique	LOD (μM)	Linear range	Real Samples	Recovery %	Ref
Fe–ZnO@PGE	Voltammetry	2.55	0.8–4.0 μM	–	–	[64]
nano-PANI:PSS	Voltammetry	51.8	0.2–0.9 mM	–	–	[10]
Fe_3O_4/MWCNT/PANI-Nafion	Voltammetry and CA	67.0	1.0–25.0 mM	Milk	97.26–98.13	[7]
GND/PANI	Voltammetry	5.0	10–90 μM	Milk based artificial matrix	–	[65]
Au/PANI-PSS hydrogel/ Urease	Voltammetry	–	10^{-4}-7 × 10^{-2} M	–	–	[66]
ITO/SG-PANI/Urs	CA	50	0.1212–3 mM	Urine	96–116	[67]
Nafion®(urease)/ PANI-Nafion®	Voltammetry	300	3–30 mM	–	–	[25]
Nf/PANI/CuF/Urs	Voltammetry	0.17	0.5–45.0 μM	Soil, milk	97–104.43	**This study**
Nf/PANI/CoF/Urs	Voltammetry	0.23	0.5–45.0 μM	–	–	**This study**
Nf/PANI/NiF/Urs	Voltammetry	0.37	0.5–45.0 μM	–	–	**This study**
Nf/PANI/ZnF/Urs	Voltammetry	0.42	0.5–45.0 μM	–	–	**This study**

PGE: Pencil graphite electrode, **PSS:** Poly(styrene sulfonate), **GND:** Graphitized nanodiamond, **Au:** Gold, **MWCNT:** Multi-Walled Carbon Nanotube, **ITO:** Indium tin oxide, **SG:** Sulfonated graphene, **CA:** Chronoamperometry.

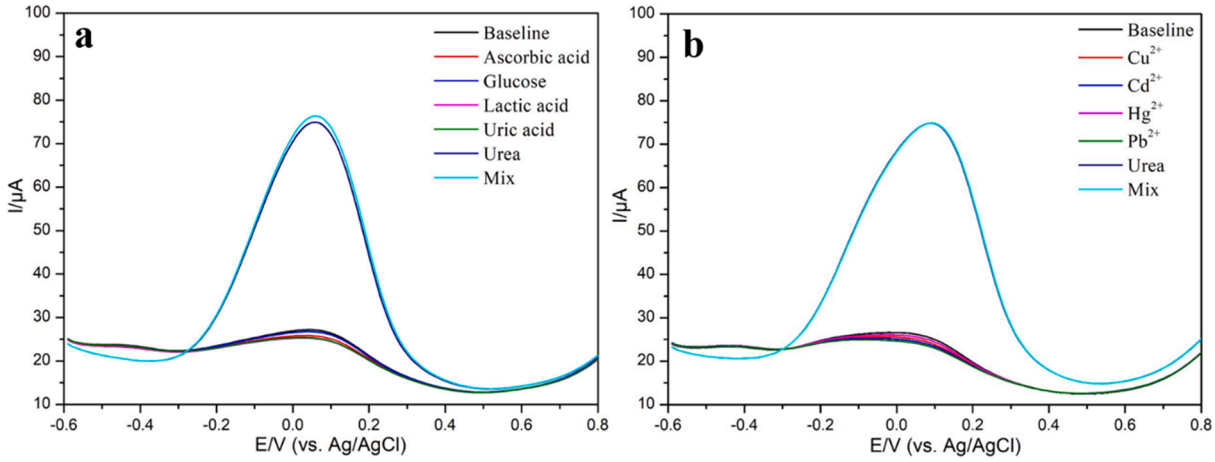

Fig. 6. DPV responses for selectivity study of Nf/PANI/CuF/Urs electrode against interfering species.

addition a mixture of agents that interfered with the presence of urea (**Fig. 6b**). The relative errors were calculated as 2.26 % and 0.78 % for organic groups and ions, respectively. Many studies were carried out in the literature for selectivity tests against urea. Wang et al. selected uric acid and glucose for selectivity test with no significant change in the peak current values in the presence of interference agents and the %RSD values were in the range of 0.7–4.36 % [70]. Bao et al. used glucose and ascorbic acid in the selectivity test. It was stated that the change in peak current was 8.89 % for glucose and 17.45 % for ascorbic acid [71]. Parsaee et al. also stated that uric, ascorbic acids, and glucose were evaluated as the main interference agents during the presence of urea therefore it was important to study these groups [72]. The above-mentioned results confirmed that the prepared biosensor (Nf/PANI/CuF/Urs) response for urea detection was reproducible and selective. It was determined from reusability experiments that it provided with a reliable data for the first three measurements.

3.5. Analysis of real samples

According to the diet, the urea concentration should be 3.0 to 6.0 mM that is tolerable urea limit as ≤ 11.0 mM [8]. Milk consumption at high urea concentration can cause various kidney function disorders, indigestion and ulcers in people [8]. In addition, nitrogen-containing fertilizers are still widely used, and therefore the presence of urea in soil and environmental water is increasing [37]. For these reasons, it is important to detect urea in food and environmental samples easily, precisely and accurately. For real sample analysis, the calculated volumes of the samples were added into the cell after the baseline determined in PBS. Thus, the amount of urea in the samples was determined, and the accuracy was determined by spike and recovery test at two different concentrations (5.0 and 7.5 μM). The recoveries are given in Table 2**.** % recovery values were calculated as 97.0 and 104.43 %. It could be stated that newly designed electrochemical biosensor (Nf/PANI/CuF/Urs) is applicable for the determination of urea in real samples with high accuracy.

Table 2
Determination of urea by Nf/PANI/CuF/Urs biosensor with DPV in soil and milk samples.

Real Samples	Added (μM)	Found (mM)[a]	Recovery (%)[b]
Soil	0	–	–
	5.00	4.85 ± 0.48	97.00
	7.50	7.65 ± 0.34	102.00
Milk	0	2.02 ± 0.21	–
	5.00	7.24 ± 0.27	104.44
	7.50	9.82 ± 0.31	104.00

[a] It was calculated by multiplying required dilution factor.
[b] Mean ± SD (n = 3).

4. Conclusions

CuF, CoF, NiF and ZnF nanoparticles were synthesized by the "co-precipitation" method in the current study. The surface of ferrit nanoparticles was modified with TEOS and APTES to obtain suitable materials for Urs enzyme immobilization. Each step was characterized and detailed information about the structures was extracted. These modified ferrite nanoparticles were comparatively evaluated with the Nf/PANI system for electrochemical detection of urea and considerable results were obtained. Among these modified ferrite nanoparticles, it was determined that CuF showed a much more sensitive electrochemical biosensor performance compared to the other ferrites. CuF demonstrated an extraordinary contribution to the increase of peak current values in electrochemical measurements due to having narrower bandgap value that was more suitable for the detection of the enzymatic degradation products of urea. As a conclusion, a new electrochemical urea biosensor which is simple, relatively inexpensive, sensitive, selective and reproducible has been developed. Thanks to the excellent features of the ferrit based biosensor, it could contribute to the perspective of new designs for enzymatic determination.

CRediT authorship contribution statement

Vildan Sanko: Data curation, Conceptualization, Methodology, Investigation, Visualization, Writing – original draft, Writing – review & editing. **Ahmet Şenocak:** Methodology, Investigation, Formal analysis, Writing – original draft. **Süreyya Oğuz Tümay:** Investigation, Software, Validation, Writing – original draft. **Erhan Demirbas:** Supervision, Investigation, Writing – original draft, Writing – review & editing.

Declaration of Competing Interest

The authors declare that they have no known competing financial interests or personal relationships that could have appeared to influence the work reported in this paper.

Data availability

No data was used for the research described in the article.

Acknowledgments

Vildan Sanko thanks TUBITAK for financial support through the TUBITAK 2211-C National Ph.D. program Scholarship Programs in the Priority Fields in Science and Technology. Also, Vildan Sanko thanks YOK 100/2000 doctorate program. This study was supported by a project from the Scientific Research Projects of Gebze Technical University (GTU-BAP, Project number: 2020-A-102-14).

References

[1] A.D. Irzalinda, J. Gunlazuardi, R. Wibowo, Development of a non-enzymatic urea sensor based on a Ni/Au electrode, IOP Publishing, pp. 012054.
[2] G.J. Kalaivani, S.K. Suja, Electroenzymatic sensing of urea using CP/MWCNT-inulin-TiO2 bioelectrode, Appl. Surf. Sci. 449 (2018) 266–276.
[3] A.A. Ibrahim, R. Ahmad, A. Umar, M.S. Al-Assiri, A.E. Al-Salami, R. Kumar, S. G. Ansari, S. Baskoutas, Two-dimensional ytterbium oxide nanodisks based biosensor for selective detection of urea, Biosens. Bioelectron. 98 (2017) 254–260.
[4] J. Das, P. Sarkar, Enzymatic electrochemical biosensor for urea with a polyaniline grafted conducting hydrogel composite modified electrode, RSC Adv. 6 (2016) 92520–92533.
[5] M. Berto, C. Diacci, L. Theuer, M. Di Lauro, D.T. Simon, M. Berggren, F. Biscarini, V. Beni, C.A. Bortolotti, Label free urea biosensor based on organic electrochemical transistors, Flexible Printed Electron. 3 (2018), 024001.
[6] S.N. Botewad, D.K. Gaikwad, N.B. Girhe, H.N. Thorat, P.P. Pawar, Urea biosensors: A comprehensive review, Biotechnol. Appl. Biochem. (2021).
[7] M. Dervisevic, E. Dervisevic, M. Şenel, Design of amperometric urea biosensor based on self-assembled monolayer of cystamine/PAMAM-grafted MWCNT/Urease, Sens. Actuators, B 254 (2018) 93–101.
[8] A.K. Singh, M. Singh, N. Verma, Electrochemical preparation of Fe3O4/MWCNT-polyaniline nanocomposite film for development of urea biosensor and its application in milk sample, J. Food Meas. Charact. 14 (2020) 163–175.
[9] B. Öndeş, F. Akpınar, M. Uygun, M. Muti, D.A. Uygun, High stability potentiometric urea biosensor based on enzyme attached nanoparticles, Microchem. J. 160 (2021), 105667.
[10] A. Soni, R.K. Surana, S.K. Jha, Smartphone based optical biosensor for the detection of urea in saliva, Sens. Actuators, B 269 (2018) 346–353.
[11] S. Uzunçar, L. Meng, A.P.F. Turner, W.C. Mak, Processable and nanofibrous polyaniline: polystyrene-sulphonate (nano-PANI: PSS) for the fabrication of catalyst-free ammonium sensors and enzyme-coupled urea biosensors, Biosens. Bioelectron. 171 (2021), 112725.
[12] W.-Q. Xie, K.-X. Yu, Y.-X. Gong, Rapid and quantitative determination of urea in milk by reaction headspace gas chromatography, Microchem. J. 147 (2019) 838–841.
[13] J. Zhang, G. Liu, Y. Zhang, Q. Gao, D. Wang, H. Liu, Simultaneous determination of ethyl carbamate and urea in alcoholic beverages by high-performance liquid chromatography coupled with fluorescence detection, J. Agric. Food. Chem. 62 (2014) 2797–2802.
[14] F. Palmas, M. Mussap, C. Fattuoni, Urine metabolome analysis by gas chromatography–mass spectrometry (GC–MS): Standardization and optimization of protocols for urea removal and short-term sample storage, Clin. Chim. Acta 485 (2018) 236–242.
[15] A. Şenocak, S.O. Tümay, E. Sarı, V. Sanko, M. Durmuş, E. Demirbas, The Simultaneously Voltammetric Determination of Spinosad and Chlorantraniliprole Pesticides by Carbazole-Ferrocene Functionalized Carbon Nanotube Architecture, J. Electrochem. Soc 168 (8) (2021), 087513, https://doi.org/10.1149/1945-7111/ac1f56.
[16] V. Sanko, A. Şenocak, S.O. Tümay, Y. Orooji, E. Demirbas, A. Khataee, An electrochemical sensor for detection of trace-level endocrine disruptor bisphenol A using Mo2Ti2AlC3 MAX phase/MWCNT composite modified electrode, Environ. Res. 212 (2022), 113071.
[17] S. Singh, M. Sharma, G. Singh, Recent advancements in urea biosensors for biomedical applications, IET Nanobiotechnol. 15 (2021) 358–379.
[18] E. Urbańczyk, M. Sowa, W. Simka, Urea removal from aqueous solutions—a review, J. Appl. Electrochem. 46 (2016) 1011–1029.
[19] G. Dhawan, G. Sumana, B.D. Malhotra, Recent developments in urea biosensors, Biochem. Eng. J. 44 (2009) 42–52.
[20] W. Hao, G. Das, H.H. Yoon, Fabrication of an amperometric urea biosensor using urease and metal catalysts immobilized by a polyion complex, J. Electroanal. Chem. 747 (2015) 143–148.
[21] M. Wang, P.-L. Tremblay, T. Zhang, Optimizing the electrical conductivity of polyacrylonitrile/polyaniline with nickel nanoparticles for the enhanced electrostimulation of Schwann cells proliferation, Bioelectrochemistry 140 (2021), 107750.
[22] J. Wang, N. Hui, Zwitterionic poly (carboxybetaine) functionalized conducting polymer polyaniline nanowires for the electrochemical detection of carcinoembryonic antigen in undiluted blood serum, Bioelectrochemistry 125 (2019) 90–96.
[23] M. Zhybak, V. Beni, M.Y. Vagin, E. Dempsey, A.P.F. Turner, Y. Korpan, Creatinine and urea biosensors based on a novel ammonium ion-selective copper-polyaniline nano-composite, Biosens. Bioelectron. 77 (2016) 505–511.
[24] M.T. Zhybak, M.Y. Vagin, V. Beni, X. Liu, E. Dempsey, A.P.F. Turner, Y.I. Korpan, Direct detection of ammonium ion by means of oxygen electrocatalysis at a copper-polyaniline composite on a screen-printed electrode, Microchim. Acta 183 (2016) 1981–1987.
[25] M.T. Zhybak, L.Y. Fayura, Y.R. Boretsky, M.V. Gonchar, A.A. Sibirny, E. Dempsey, A.P.F. Turner, Y.I. Korpan, Amperometric L-arginine biosensor based on a novel recombinant arginine deiminase, Microchim. Acta 184 (2017) 2679–2686.
[26] Y.-C. Luo, J.-S. Do, Urea biosensor based on PANi (urease)-Nafion®/Au composite electrode, Biosens. Bioelectron. 20 (2004) 15–23.
[27] P.A. Vinosha, A. Manikandan, A.C. Preetha, A. Dinesh, Y. Slimani, M.A. Almessiere, A. Baykal, B. Xavier, G. Nirmala, Review on recent advances of synthesis, magnetic properties, and water treatment applications of cobalt ferrite nanoparticles and nanocomposites, J. Supercond. Novel Magn. 34 (2021) 995–1018.
[28] T.F. Marinca, I. Chicinaş, O. Isnard, Structural and magnetic properties of the copper ferrite obtained by reactive milling and heat treatment, Ceram. Int. 39 (2013) 4179–4186.
[29] S.R. Mokhosi, W. Mdlalose, A. Nhlapo, M. Singh, Advances in the Synthesis and Application of Magnetic Ferrite Nanoparticles for Cancer Therapy, Pharmaceutics 14 (2022) 937.
[30] K. Asadpour-Zeynali, F. Mollarasouli, Novel electrochemical biosensor based on PVP capped CoFe2O4@ CdSe core-shell nanoparticles modified electrode for ultra-trace level determination of rifampicin by square wave adsorptive stripping voltammetry, Biosens. Bioelectron. 92 (2017) 509–516.
[31] K.K. Kefeni, T.A.M. Msagati, B.B. Mamba, Ferrite nanoparticles: synthesis, characterisation and applications in electronic device, Mater. Sci. Eng., B 215 (2017) 37–55.
[32] V. Sanko, A. Şenocak, S. Oğuz Tümay, T. Çamurcu, E. Demirbas, Core-shell Hierarchical Enzymatic Biosensor Based on Hyaluronic Acid Capped Copper Ferrite Nanoparticles for Determination of Endocrine-disrupting Bisphenol A, Electroanalysis 34 (2022) 561–572.
[33] X. Sun, L. Zhang, X. Zhang, X. Liu, J. Jian, D. Kong, D. Zeng, H. Yuan, S. Feng, Electrochemical dopamine sensor based on superionic conducting potassium ferrite, Biosens. Bioelectron. 153 (2020), 112045.
[34] M.A.A. Kerroum, A. Essyed, C. Iacovita, W. Baaziz, D. Ihiawakrim, O. Mounkachi, M. Hamedoun, A. Benyoussef, M. Benaissa, O. Ersen, The effect of basic pH on the elaboration of ZnFe2O4 nanoparticles by co-precipitation method: Structural, magnetic and hyperthermia characterization, J. Magn. Magn. Mater. 478 (2019) 239–246.
[35] S.A. Kulkarni, P.S. Sawadh, P.K. Palei, Synthesis and characterization of superparamagnetic Fe 3 O 4@ SiO 2 nanoparticles, J. Korean Chem. Soc. 58 (2014) 100–104.
[36] J. Nonkumwong, P. Pakawanit, A. Wipatanawin, P. Jantaratana, S. Ananta, L. Srisombat, Synthesis and cytotoxicity study of magnesium ferrite-gold core-shell nanoparticles, Mater. Sci. Eng., C 61 (2016) 123–132.
[37] T. Alizadeh, M.R. Ganjali, F. Rafiei, Trace level and highly selective determination of urea in various real samples based upon voltammetric analysis of diacetylmonoxime-urea reaction product on the carbon nanotube/carbon paste electrode, Anal. Chim. Acta 974 (2017) 54–62.
[38] S.F. Mansour, O.M. Hemeda, S.I. El-Dek, B.I. Salem, Influence of La doping and synthesis method on the properties of CoFe2O4 nanocrystals, J. Magn. Magn. Mater. 420 (2016) 7–18.
[39] A. Antonello, G. Jakob, P. Dolcet, R. Momper, M. Kokkinopoulou, K. Landfester, R. Munoz-Espi, S. Gross, Synergy of miniemulsion and solvothermal conditions for the low-temperature crystallization of magnetic nanostructured transition-metal ferrites, Chem. Mater. 29 (2017) 985–997.
[40] N. Güy, M. Özacar, Visible light-induced degradation of indigo carmine over ZnFe2O4/Tannin/ZnO: role of tannin as a modifier and its degradation mechanism, Int. J. Hydrogen Energy 43 (2018) 8779–8793.
[41] A.C.B. Jesus, J.R. Jesus, R.J.S. Lima, K.O. Moura, J.M.A. Almeida, J.G.S. Duque, C. T. Meneses, Synthesis and magnetic interaction on concentrated Fe3O4 nanoparticles obtained by the co-precipitation and hydrothermal chemical methods, Ceram. Int. 46 (2020) 11149–11153.
[42] X. Wu, W. Wang, F. Li, S. Khaimanov, N. Tsidaeva, M. Lahoubi, PEG-assisted hydrothermal synthesis of CoFe2O4 nanoparticles with enhanced selective adsorption properties for different dyes, Appl. Surf. Sci. 389 (2016) 1003–1011.
[43] M. Yamaura, R.L. Camilo, L.C. Sampaio, M.A. Macedo, M. Nakamura, H.E. Toma, Preparation and characterization of (3-aminopropyl) triethoxysilane-coated magnetite nanoparticles, J. Magn. Magn. Mater. 279 (2004) 210–217.
[44] M. Gharagozlou, Synthesis, characterization and influence of calcination temperature on magnetic properties of nanocrystalline spinel Co-ferrite prepared by polymeric precursor method, J. Alloy. Compd. 486 (2009) 660–665.
[45] A.D. Patil, R.A. Pawar, S.M. Patange, S.S. Jadhav, S.K. Gore, S.E. Shirsath, S.S. Meena, TiO2-Doped Ni0. 4Cu0. 3Zn0. 3Fe2O4 Nanoparticles for Enhanced Structural and Magnetic Properties, ACS omega, 6 (2021) 17931-17940.
[46] M. Gao, W. Li, J. Dong, Z. Zhang, B. Yang, Synthesis and characterization of superparamagnetic Fe3O4@ SiO2 core-shell composite nanoparticles, World Journal of, Condens. Matter Phys. 1 (2011) 49–54.
[47] W. Huang, X. Yang, S. Zhao, M. Zhang, X. Hu, J. Wang, H. Zhao, Fast and selective recognizes polysaccharide by surface molecularly imprinted film coated onto aldehyde-modified magnetic nanoparticles, Analyst 138 (2013) 6653–6661.
[48] M. Barisik, S. Atalay, A. Beskok, S. Qian, Size dependent surface charge properties of silica nanoparticles, The Journal of Physical Chemistry C 118 (2014) 1836–1842.
[49] S. Swathi, R. Yuvakkumar, P.S. Kumar, G. Ravi, D. Velauthapillai, Annealing temperature effect on cobalt ferrite nanoparticles for photocatalytic degradation, Chemosphere 281 (2021), 130903.

[50] Y. Cheng, L. He, G. Xia, C. Ren, Z. Wang, Nanostructured gC 3 N 4/AgI composites assembled by AgI nanoparticles-decorated gC 3 N 4 nanosheets for effective and mild photooxidation reaction, New J. Chem. 43 (2019) 14841–14852.
[51] S.M. Nia, F. Kheiri, E. Jannatdoust, M. Sirousazar, V.A. Chianeh, G. Kheiri, A Highly Sensitive Non-Enzymatic Urea Sensor Based on Ni (OH) 2/Mn3O4/rGO/PANi Nanocomposites Using Screen-Printed Electrodes, J. Electrochem. Soc. 168 (2021), 067504.
[52] J. Li, J. Zhang, J.-H. Yang, Research progress and applications of nickel-based catalysts for electrooxidation of urea, Int. J. Hydrogen Energy (2021).
[53] V. Kumar, I. Kaur, S. Arora, R. Mehla, K. Vellingiri, K.-H. Kim, Graphene nanoplatelet/graphitized nanodiamond-based nanocomposite for mediator-free electrochemical sensing of urea, Food Chem. 303 (2020), 125375.
[54] S. Hussain, S.-Y. Park, Sweat-Based Noninvasive Skin-Patchable Urea Biosensors with Photonic Interpenetrating Polymer Network Films Integrated into PDMS Chips, ACS Sensors 5 (2020) 3988–3998.
[55] R.K. Srivastava, S. Srivastava, T.N. Narayanan, B.D. Mahlotra, R. Vajtai, P. M. Ajayan, A. Srivastava, Functionalized multilayered graphene platform for urea sensor, ACS Nano 6 (2012) 168–175.
[56] M. Hosseinian, G.N. Darzi, A. Rahimpour, A novel bioelectrochemical sensor based on immobilized urease on the surface of nickel oxide nanoparticle and polypyrrole composite modified Pt electrode, Electroanalysis 31 (2019) 2530–2537.
[57] W. Wang, W. Wang, J.J. Davis, X. Luo, Ultrasensitive and selective voltammetric aptasensor for dopamine based on a conducting polymer nanocomposite doped with graphene oxide, Microchim. Acta 182 (2015) 1123–1129.
[58] R. Rahmanian, S.A. Mozaffari, H.S. Amoli, M. Abedi, Development of sensitive impedimetric urea biosensor using DC sputtered Nano-ZnO on TiO2 thin film as a novel hierarchical nanostructure transducer, Sens. Actuators, B 256 (2018) 760–774.
[59] R. Rahmanian, S.A. Mozaffari, M. Abedi, Disposable urea biosensor based on nanoporous ZnO film fabricated from omissible polymeric substrate, Mater. Sci. Eng., C 57 (2015) 387–396.
[60] A. Şenocak, S.O. Tümay, İ. Ömeroğlu, V. Şanko, Crosslinker polycarbazole supported magnetite MOF@ CNT hybrid material for synergetic and selective voltammetric determination of adenine and guanine, J. Electroanal. Chem. 905 (2022), 115963.
[61] S.O. Tümay, A. Şenocak, E. Sarı, V. Şanko, M. Durmuş, E. Demirbas, A new perspective for electrochemical determination of parathion and chlorantraniliprole pesticides via carbon nanotube-based thiophene-ferrocene appended hybrid nanosensor, Sens. Actuators, B 345 (2021), 130344.
[62] H.R. Jamei, B. Rezaei, A.A. Ensafi, Ultra-sensitive and selective electrochemical biosensor with aptamer recognition surface based on polymer quantum dots and C60/MWCNTs-polyethylenimine nanocomposites for analysis of thrombin protein, Bioelectrochemistry 138 (2021), 107701.
[63] Q. Huang, X. Lin, L. Tong, Q.-X. Tong, Graphene quantum dots/multiwalled carbon nanotubes composite-based electrochemical sensor for detecting dopamine release from living cells, ACS Sustainable Chem. Eng. 8 (2020) 1644–1650.
[64] K.K. Kefeni, T.A.M. Msagati, T.T.I. Nkambule, B.B. Mamba, Spinel ferrite nanoparticles and nanocomposites for biomedical applications and their toxicity, Mater. Sci. Eng., C 107 (2020), 110314.
[65] D. Dhinasekaran, P. Soundharraj, M. Jagannathan, A.R. Rajendran, S. Rajendran, Hybrid ZnO nanostructures modified graphite electrode as an efficient urea sensor for environmental pollution monitoring, Chemosphere 296 (2022), 133918.
[66] V. Kumar, R. Mahajan, I. Kaur, K.-H. Kim, Simple and mediator-free urea sensing based on engineered nanodiamonds with polyaniline nanofibers synthesized in situ, ACS Appl. Mater. Interfaces 9 (2017) 16813–16823.
[67] A. Słoniewska, B. Pałys, Supramolecular polyaniline hydrogel as a support for urease, Electrochim. Acta 126 (2014) 90–97.
[68] G. Das, H.H. Yoon, Amperometric urea biosensors based on sulfonated graphene/polyaniline nanocomposite, Int. J. Nanomed. 10 (2015) 55.
[69] F. Colmati, L.F. Sgobbi, G.F. Teixeira, R.S. Vilela, T.D. Martins, G.O. Figueiredo, Electrochemical biosensors containing pure enzymes or crude extracts as enzyme sources for pesticides and phenolic compounds with pharmacological property detection and quantification, Biosensors for Environmental Monitoring, IntechOpen2019.
[70] Y. Wang, Y. Zhang, Y. Wang, R. Zhu, Y. Chen, X. Liu, J. Xu, M. Li, D. Wang, Urea detection of electrochemical transistor sensors based on polyanline (PANI)/MWCNT/cotton yarns, Electroanalysis 33 (2021) 2406–2416.
[71] Q. Bao, Z. Yang, Y. Song, M. Fan, P. Pan, J. Liu, Z. Liao, J. Wei, Printed flexible bifunctional electrochemical urea-pH sensor based on multiwalled carbon nanotube/polyaniline electronic ink, J. Mater. Sci.: Mater. Electron. 30 (2019) 1751–1759.
[72] Z. Parsaee, Synthesis of novel amperometric urea-sensor using hybrid synthesized NiO-NPs/GO modified GCE in aqueous solution of cetrimonium bromide, Ultrason. Sonochem. 44 (2018) 120–128.